JPE 17-4-20

https://doi.org/10.6113/JPE.2017.17.4.1048
ISSN(Print): 1598-2092 / ISSN(Online): 2093-4718

PWM-based Integral Sliding-mode Controller for Unity Input Power Factor Operation of Indirect Matrix Converter

Lazhar Rmili[*], Mahmoud Hamouda[**], Salem Rahmani[†], Handy Fortin Blanchette[***], and Kamal Al-Haddad[***]

[†,*]Laboratory of Biophysics and Medical Technology, ISTMT, Tunis El-Manar University, Tunis, Tunisia
[**]Laboratory of Advanced Technology and Intelligent Systems, ENISo, Sousse University, Sousse, Tunisia
[***]Canada Research Chair in Energy Conversion and Power Electronics, ETS of Montreal, Quebec, Canada

Abstract

An indirect matrix converter (IMC) is a modern power generation system that enables a direct ac/ac conversion without the need for any bulky and limited lifetime electrolytic capacitor. This system also allows four-quadrant operation, generation of sinusoidal output voltage waveforms with variable frequency and amplitude, and control of input power factor. This study proposes a pulse-width modulation-based sliding-mode controller to achieve unity input-power factor operation of the IMC independently of the active power exchanged with the grid, as well as a fast dynamic response. The designed equivalent control law determines, at each sampling period, the appropriate q-axis component of the modulated input current to be injected into the grid through the LC input filter. An integral term of the error is included in the expression of the sliding surface to increase the accuracy of the control method. A double space vector modulation method is used to synthesize the direction of the space vector of the input currents as required by the sliding-mode controller and the space vectors of the target output voltages. Simulation and experimental results are provided to show the effectiveness and evaluate the performance of the proposed control method.

Key words: Ac/ac conversion, Grid-connected converters, Matrix converter, Power factor correction, Power quality, Sliding-mode control, Space vector modulation

NOMENCLATURE

d_{1I}, d_{2I}	Duty cycles applied to synthesize the space vector of output voltages
d_{1R}, d_{2R}	Duty cycles applied to synthesize the space vector direction of input currents
$E_{a,b,c}$	Instantaneous grid voltages in abc frame
$\bar{E}$	Space vectors of grid voltages
$E_{d,q}$	d-q components of $E_{a,b,c}$ expressed in a synchronous reference frame
$i_{ma,mb,mc}$	Instantaneous input currents in abc frame
$\bar{I}_m^*$	Space vector of target input currents
$i_{md,mq}$	d-q components of input currents $i_{ma,mb,mc}$
$i_{sa,sb,sc}$	Instantaneous line currents in abc frame
$\bar{I}_s$	Space vector of line currents
$i_{sd,sq}$	d-q components of $i_{sa,sb,sc}$
L, c, r	Inductance, capacitance, and resistance of input filter, respectively
V_{dc}	Virtual dc-link voltage
$\langle V_{dc} \rangle$	Estimated average value of the dc-link voltage
$V_{ma,mb,mc}$	Voltages across the input filter capacitors
$V_{md,mq}$	d-q components of $V_{ma,mb,mc}$
i_{dc}	dc-link current
$i_{A,B,C}$	Load currents
$V_{A,B,C}$	Output voltages

Manuscript received Mar. 14, 2016; accepted Feb. 17, 2017
Recommended for publication by Associate Editor Sangshin Kwak.
[†]Corresponding Author: rsalem02@yahoo.fr
Tel: +216-71-496-066, Fax: +216 -71-391-166, Tunis El-Manar Univ.
[*]Laboratory of Biophysics and Medical Technology, ISTMT, Tunis El-Manar University,Tunisia
[**]Laboratory of Advanced Technology and Intelligent Systems, ENISo, Sousse University, Tunisia
[***]Canada Research Chair in Energy Conversion and Power Electronics. ETS of Montreal, Canada

$\bar{V}^*$	Space vector of target output voltages
$V_{d,q}$	d-q components of $V_{A,B,C}$
φ_i	Phase angle between $\bar{E}$ and $\bar{I}_m^*$
$\bar{\gamma}_i$	Phase angle of $\bar{I}_m^*$ within its operating sector
ω	Angular frequency of grid voltage
ω_0	Resonant angular frequency of input filter
$S_{x(x=A,B,C)}$	Switching states of the inverter stage
$S_{x(x=a,b,c)}$	Switching states of the rectifier stage

I. INTRODUCTION

Matrix converters are ac–ac static power conversion devices without dc-link energy storage elements. They offer attractive features, such as variable amplitude and frequency voltages that are generated at the load side, sinusoidal input/output currents, controllable input power factor, and regenerative capability. The lack of bulky and limited-lifetime electrolytic capacitors in this all-silicon topology allows the construction of a more compact and reliable converter. No sensors or control schemes are needed to regulate the voltage across the dc-link capacitor in contrast to the conventional back-to-back converter that requires them [1]. Matrix converters have recently attracted significant attention from researchers and have become increasingly attractive for applications of military power supplies, wind energy conversion, and induction motor drives, especially in terms of reliability, efficiency, and current or voltage distortion improvement. The indirect matrix converter (IMC) topology introduced in 2001 has the same performance as the conventional direct matrix converter (DMC), while reducing the commutation problem and control complexity. The IMC illustrated in Fig. 1 consists of a four-quadrant rectifier stage cascaded with a two-level inverter stage. The rectifier stage provides a positive dc-link voltage and sinusoidal input currents. The inverter stage generates the target ac output voltages. An LC low-pass filter is connected between the input stage of the converter and the grid to compensate for the high frequency harmonics of the modulated input currents and mitigate the overvoltage caused by the commutation process.

Many modulation algorithms have been suggested in the literature over the last few years. Most of them are developed using the double-space vector modulation (DSVM) technique [2]-[5], the carrier-based sine pulse-width modulation (PWM) method [6]-[8], and a hybrid PWM [9] algorithm. These modulation schemes were developed with the aim to produce variable amplitude, variable frequency output voltages, and unity input power factor (UIPF). Given that these algorithms operate in an open-loop setting, they can control only the instantaneous phase angle of the modulated input currents $i_{ma,mb,mc}$. However, a phase angle arises between the line currents $i_{sa,sb,sc}$ and the grid voltage waveforms E_{abc} due to the presence of input filter. Undesirable line current oscillations also occur during the transient operations of the converter. The input filter elements are generally sized to achieve UIPF at full-loading condition. Consequently, the input power factor decreases as the active power demanded from the load decreases [9], [10].

Many control methods were proposed to effectively maintain near UIPF even under variable active power exchanged between the grid and the load. A combined symmetric and asymmetric modulation method of the conventional matrix converter topology was proposed in [11] to enable online compensation for the displacement factor introduced by the input filter. Nevertheless, this method operates in an open loop, which leads to a poor dynamic performance, and it is sensitive to the variation of in input filter parameters. In [12], a direct space vector modulation method and a proportional–integral (PI) controller were implemented to achieve UIPF operation of the conventional matrix converter topology. In [13], a simple PI controller was proposed to control the input power factor of an ac/dc matrix rectifier. However, no compensation for grid voltage, input filter capacitor voltage, and active current dynamics was considered in both references [12] and [13]. In [14], a predictive control scheme was applied with the IMC topology. Nonetheless, the proposed approach was tested under steady-state condition and constant active power operation only. In [15], an input–output feedback linearization-based control method was applied with the IMC to achieve UIPF, but no experimental results were provided to validate the proposed approach. In [16], a direct sliding-mode controller based on the space vector representation of the switching states of the converter was implemented on the DMC topology. Nevertheless, this method cannot be applied with the IMC topology commutating at zero dc-link current. Indeed, this safe commutation strategy needs the determination of the switching patterns for both conversion stages at the beginning of each switching period. On the contrary, the conventional sliding-mode control (SMC) offers many advantages, such as simpler implementation, robustness against parameter variation, and a finite reaching time [17], [18]. However, its implementation on power converters leads to a high and variable switching frequency operation [19]. This condition increases the power losses and the conducted and radiated emission levels in the vicinity of the converter [20], and it also makes the electromagnetic interference (EMI) filter design difficult.

This study proposes a PWM-based SMC method to achieve UIPF operation of the IMC independently of the active power exchanged with the grid, as well as a fast dynamic response. The designed equivalent control law determines, at each sampling period, the appropriate q-axis component of the modulated input current to be injected into the grid through the LC input filter. An integral term of the error is included in the expression of the sliding surface to increase the accuracy of the control method. This technique operates at a fixed switching frequency, which makes it suitable for a real-time

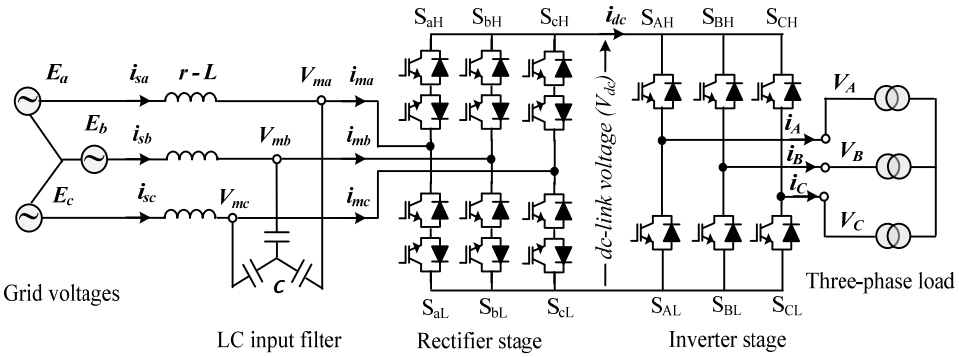

Fig. 1. Power circuit of an IMC.

implementation on digital processors and reduces the complexity of EMI filter design.

A DSVM method is used to synthesize the direction of the space vector of input currents as required by the sliding mode controller and the space vector of target output voltages. The effectiveness of the proposed control method in achieving UIPF operation is confirmed by the simulation and experimental results.

II. Review of DSVM Algorithm

The DSVM technique synthesizes two space vectors that are equivalent to the target three-phase input currents (i_{ma}, i_{mb}, i_{mc}) and output voltages (V_A, V_B, V_C) at each switching period [4]. The algorithm is better understood by referring to Figs. 2(a-b) and 3. In the figures, the space vectors of input current and output voltage ($\bar{I}_m^*$ and $\bar{V}^*$) are both located within sector 1 of the complex plane. At each switching period, the reference vector of input current $\bar{I}_m^*$ is modulated by impressing its two adjacent active vectors $\bar{I}_1$ and $\bar{I}_2$ by the duty cycles, namely, d_{1R} and d_{2R}, respectively, as depicted in Fig. 2(a). Therefore, S_{aH} is turned on over the full-switching period, and S_{bL} and S_{cL} are modulated complementarily to the dead time. Their relative turn-on times are d_{1R} and d_{2R} (Fig. 3). The remaining four-quadrant switches S_{aL}, S_{bH}, and S_{cH} are therefore not gated. The expressions of duty cycles d_{1R} and d_{2R} are given in Equ. (1), where $\bar{\gamma}_i$ is the phase angle of the space vector $\bar{I}_m^*$ within its respective operating sector [4].

$$d_{1R} = \frac{\sin\left(\frac{\pi}{3} - \bar{\gamma}_i\right)}{\cos\left(\frac{\pi}{6} - \bar{\gamma}_i\right)}, \qquad d_{2R} = \frac{\sin\left(\bar{\gamma}_i\right)}{\cos\left(\frac{\pi}{6} - \bar{\gamma}_i\right)} \tag{1}$$

This commutation sequence of the rectifier stage switches gives rise to two different values of the dc-link voltage, namely, E_{ab} and $-E_{ca}$. To compensate for the effect of this continuous change of dc-link voltage on the load side waveforms, two time intervals should be considered to obtain the switching pattern of the inverter stage.

In the first time interval, where the dc-link voltage is equal to E_{ab}, the reference vector of output voltage $\bar{V}^*$ is modulated during the relative time d_{1R} by impressing its two adjacent

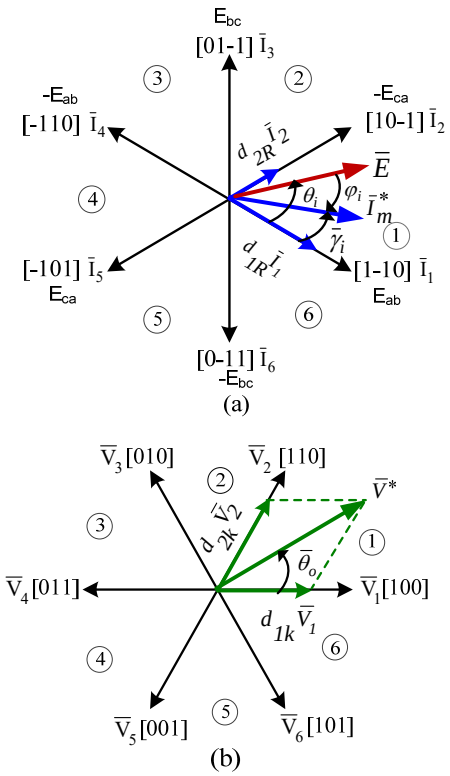

Fig. 2. DSVM of IMC: (a) synthesis of $\bar{I}_m^*$ - (b) synthesis of $\bar{V}^*$ (k =1,2).

active vectors ($\bar{V}_1$, $\bar{V}_2$) and zero vectors ($\bar{V}_0$, $\bar{V}_7$), with the appropriate duty cycles d_{11}, d_{12}, and d_{10}, as illustrated in Fig. 2(b).

As for the second time interval, where the dc-link voltage is equal to $-E_{ca}$, $\bar{V}^*$ is modulated again during the relative time d_{2R} by impressing the same adjacent active vectors ($\bar{V}_1$, $\bar{V}_2$) and zero vectors ($\bar{V}_0$, $\bar{V}_7$), with the appropriate duty cycles d_{21}, d_{22}, and d_{20}, as illustrated in Fig. 2(b).

The expressions of duty cycles d_{11}, d_{12}, d_{10}, d_{21}, d_{22}, and d_{20} are given as follows [4]:

$$\begin{cases} d_{11} = d_{1R}d_{1I}, d_{12} = d_{1R}d_{2I}, d_{10} = d_{1R} - (d_{11} + d_{12}) \\ d_{21} = d_{2R}d_{1I}, d_{22} = d_{2R}d_{2I}, d_{20} = d_{2R} - (d_{21} + d_{22}) \end{cases} \tag{2}$$

The expressions of d_{1I} and d_{2I} are as follows [1]:

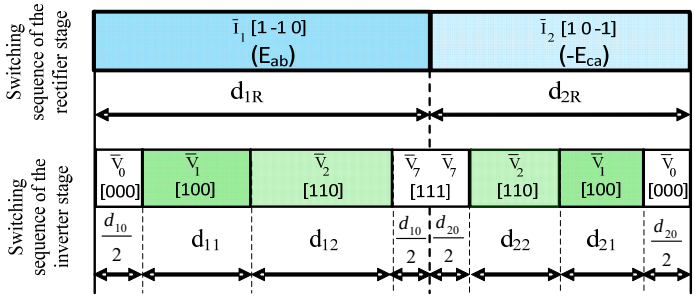

Fig. 3. Switching patterns when the reference vectors of output voltage and input current are both located within sectors 1 of the complex plane.

$$\begin{cases} d_{1I} = \frac{\sqrt{3}\ |\bar{V}^*|}{\langle V_{dc}\rangle} sin\left(\frac{\pi}{3} - \bar{\theta}_o\right) \\ d_{2I} = \frac{\sqrt{3}\ |\bar{V}^*|}{\langle V_{dc}\rangle} sin\left(\bar{\theta}_o\right) \end{cases} \quad (3)$$

where $\langle V_{dc}\rangle$ is the local average value of the dc-link voltage computed over a switching period [1]. $\bar{\theta}_o$ is the phase angle of the output voltage space vector within its operation sector. Fig. 3 illustrates the switching patterns of the rectifier and inverter stages that correspond to the operation case of Figs. 2(a-b) [21].

III. Modeling of Converter

A. Modeling of Converter in abc Reference Frame

The mathematical relationship in the abc stationary reference frame between the currents and voltages at the input and output terminals of the converter is formulated as follows:

$$[V_A \quad V_B \quad V_C]^T = [S_A \quad S_B \quad S_C]^T V_{dc} \quad (4)$$

$$[i_{ma} \quad i_{mb} \quad i_{mc}]^T = [S_a \quad S_b \quad S_c]^T i_{dc} \quad (5)$$

where $V_{A,B,C}$ are the output voltages across the output terminals of the converter. $S_{x(x=A,B,C)}$ are the switching states of the inverter stage; $S_{x(x=A,B,C)} = 1$ when the upper switch of the leg $x\ (x = A, B, C)$ is on state. Otherwise, $S_{x(x=A,B,C)} = -1$. $i_{ma,mb,mc}$ are the input currents provided by the rectifier stage and injected into the grid through the LC input filter. $S_{x(x=a,b,c)}$ are the switching states of the rectifier stage. $S_{x(x=a,b,c)} = 1$ when the upper switch of the leg $x\ (x = a, b, c)$ is on state. $S_{x(x=a,b,c)} = -1$ when the lower switch of the leg x is on state. Otherwise, $S_{x(x=a,b,c)} = 0$. i_{dc} and V_{dc} are the current and voltage across the virtual dc-link, respectively. Their instantaneous expressions are derived as follows:

$$V_{dc} = [S_a \quad S_b \quad S_c][V_{ma} \quad V_{mb} \quad V_{mc}]^T \quad (6)$$

$$i_{\boldsymbol{dc}} = [S_A \quad S_B \quad S_C][i_A \quad i_B \quad i_C]^{\boldsymbol{T}} \quad (7)$$

where $V_{ma,mb,mc}$ are the voltages across the input filter capacitors, and $i_{A,B,C}$ are the load currents. The dynamics of the line currents and voltages across the input filter capacitors are also expressed in the abc reference frame as follows:

$$\frac{d}{dt}[i_{sa} \quad i_{sb} \quad i_{sc}]^T = -\frac{r}{L}[i_{sa} \quad i_{sb} \quad i_{sc}]^T + \frac{1}{3L}[K][E_{sa} \quad E_{sb} \quad E_{sc}]^T - \frac{1}{3L}[K][V_{ma} \quad V_{mb} \quad V_{mc}]^T \quad (8)$$

$$\frac{d}{dt}[V_{ma} \quad V_{mb} \quad V_{mc}]^T = \frac{1}{c}[i_{sa} \quad i_{sb} \quad i_{sc}]^T - \frac{1}{c}[i_{ma} \quad i_{mb} \quad i_{mc}]^T \quad (9)$$

where $i_{sa,sb,sc}$ and $E_{a,b,c}$ are the line currents and grid voltages, respectively. $V_{ma,mb,mc}$ are the voltages across the LC input filter. r, L, and c are the input filter resistance, inductance, and capacitance, respectively. The matrix K is defined as follows:

$$K = \frac{1}{3}\begin{bmatrix} 2 & -1 & -1 \\ -1 & 2 & -1 \\ -1 & -1 & 2 \end{bmatrix} \quad (10)$$

B. Average Model in Two d-q Reference Frames

Reporting the input and output variables into two rotating dq reference frames synchronized with the grid and output voltages, respectively. The switching states of each converter are replaced with the corresponding duty cycles applied to synthesize the input current or output voltage space vectors. Thereafter, the dynamics of the line currents and the capacitor voltages of input filter are derived as follows:

$$\begin{cases} \frac{d}{dt} i_{sd} = -\frac{r}{L} i_{sd} + \omega i_{sq} + \frac{E_d}{L} - \frac{V_{md}}{L} \\ \frac{d}{dt} i_{sq} = -\frac{r}{L} i_{sq} - \omega i_{sd} + \frac{E_q}{L} - \frac{V_{mq}}{L} \\ \frac{d}{dt} V_{md} = \omega V_{mq} + \frac{1}{c} i_{sd} - \frac{1}{c} i_{md} \\ \frac{d}{dt} V_{mq} = -\omega V_{md} + \frac{1}{c} i_{sq} - \frac{1}{c} i_{mq} \end{cases} \quad (11)$$

The d-q components of input currents and output voltages are expressed as follows:

$$\begin{cases} i_{md} = \sqrt{2}\langle i_{dc}\rangle \left(d_{1R} \cos \bar{\gamma}_i + d_{2R} \cos\left(\bar{\gamma}_i - \frac{\pi}{3}\right)\right) \\ i_{mq} = -\sqrt{2}\langle i_{dc}\rangle \left(d_{1R} \sin \bar{\gamma}_i + d_{2R} \sin\left(\bar{\gamma}_i - \frac{\pi}{3}\right)\right) \end{cases} \quad (12)$$

$$\begin{cases} V_d = \sqrt{\frac{2}{3}}\langle V_{dc}\rangle \left(d_{1I} \cos \bar{\theta}_o + d_{2I} \cos\left(\bar{\theta}_o - \frac{\pi}{3}\right)\right) \\ V_q = -\sqrt{\frac{2}{3}}\langle V_{dc}\rangle \left(d_{1I} \sin \bar{\theta}_o + d_{2I} \sin\left(\bar{\theta}_o - \frac{\pi}{3}\right)\right) \end{cases} \quad (13)$$

where $d_{1I} = d_{11} + d_{12}, and\ d_{2I} = d_{21} + d_{22}$.
i_{sd} and i_{sq} are the d-q components of the line currents $i_{sa,sb,sc}$. V_{md} and V_{mq} are the d-q components of the voltages

across the LC input filter. E_d and E_q are the d-q components of the grid voltages $E_{a,b,c}$. V_d and V_q are the d-q components of the output voltages $V_{A,B,C}$. i_{md} and i_{mq} are the d-q components of the input currents $i_{ma,mb,mc}$ that are considered control laws. $\bar{\gamma}_i$ and $\bar{\theta}_o$ are the phase angles within their respective operating sectors of the space vectors of input currents and output voltages, as depicted in Figs. 2 (a-b). $\langle V_{dc} \rangle$ and $\langle i_{dc} \rangle$ are the average values over a switching period of the dc-link voltage and current.

IV. Design of Proposed PWM Integral Sliding-Mode Controller

A. Preliminaries

The conventional SMC determines only one switching state at any switching period to drive any state variable x to reach a predesigned sliding surface in a finite time and remain on it until reaching the equilibrium point. This technique is robust; however, when applied with power converters, it leads to a high and non-constant switching frequency operation. This condition increases the conducted and radiated disturbance levels and makes the EMI filter design difficult. The PWM-based sliding-mode controller, which operates at a fixed switching frequency, determines an equivalent control law, namely, u_{eq}, at any sampling time [20], [22]. Thereafter, this control law is applied at the input of a PWM modulator, which generates a combination of switching states with appropriate duration to synthesize u_{eq} in an average sense. This feature makes the controller suitable for real-time implementation on digital processors. This controller also reduces the problems related to EMC and makes the EMI filter design simpler. For these reasons, this controller is adopted in this study. As this type of sliding-mode controller operates in a similar manner as a discrete-time or quasi-sliding-mode controller, its implementation is performed through the following two steps [23]:

- An appropriate switching function is designed, such that the sliding mode on the sliding surface remains stable.
- A control law that satisfies a reaching condition is determined. This law implies that when a state variable x starts from its initial state, it crosses over the switching surface in a finite number of sampling periods and remains within a quasi-sliding-mode band until it reaches the equilibrium point.

B. Controller Design

The objective of this section is to design a PWM-sliding-mode controller that maintains close to zero in an average sense of the q-axis component of the line current (i_{sq}) while ensuring a fast dynamic response. The control law is the q-axis component of the input current (i_{mq}) modulated by the rectifier stage. The state variable is defined as $x_1 = i_{sq}$, and the equivalent control law is $u_{eq} = i_{mq}$. Equ. (11) indicates that u_{eq} does not appear in the first derivative of x_1 ($\dot{x}_1 = \frac{d}{dt} i_{sq}$). Therefore, we should differentiate many times the state variable x_1 until the control law u_{eq} appears in the dynamics of x_1. By doing so, we obtain the following controllable form of the canonical model, where the equivalent control law appears in the second derivative of x_1:

$$\begin{cases} \dot{x}_1 = x_2 \\ \dot{x}_2 = x_1\left(\left(\frac{r}{L}\right)^2 - \omega^2 - \omega_0^2\right) + i_{sd}\left(\frac{2r}{L}\omega\right) + E_d\left(-\frac{\omega}{L}\right) \\ \quad + V_{md}\left(\frac{2\omega}{L}\right) + E_q\left(-\frac{r}{L^2}\right) + V_{mq}\left(\frac{r}{L^2}\right) + \frac{1}{L}\frac{d}{dt}E_q + \omega_0^2 i_{mq} \end{cases} \quad (14)$$

where $\omega_0^2 = \frac{1}{Lc}$.

As the relative degree of x_1 dynamics is equal to two, a first-order sliding surface can be defined as follows:

$$S(t) = c_1 \dot{e} + c_2\, e = 0 \quad (15a)$$

where $e = x_{1ref} - x_1 = i_{sqref} - i_{sq}$, and c_1, c_2 are positive sliding constants. However, the sliding surface given in Equ. (15a) does not lead to a zero steady-state error [20], [24]. Therefore, an integral term is added to the expression of the sliding function $S(t)$, such that

$$S(t) = c_1 \dot{e} + c_2\, e + c_3 \int e = 0 \quad (15b)$$

The adopted reaching law that enables the error dynamics to cross the switching function in a finite time is

$$\dot{S}(t) = -qS(t) - \varepsilon\, Sgn(S) \quad (16)$$

where q and ε are two positive and constant terms.

Replacing Equ. (15b) with Equ. (16) leads to

$$c_1 \ddot{e} + c_2 \dot{e} + c_3 e = -q(c_1 \dot{e} + c_2 e + c_3 \int e) - \varepsilon\, Sgn(S) \quad (17)$$

Developing Equ. (17) and arranging the terms lead to the following expression of the equivalent control law u_{eq}:

$$u_{eq} = i_{mq} = \frac{1}{\omega_0^2}\begin{bmatrix} x_1\left(\omega^2 + \omega_0^2 - \left(\frac{r}{L}\right)^2 + \left(\frac{c_2}{c_1} + q\right)\frac{r}{L} - \left(\frac{c_3}{c_1} + q\frac{c_2}{c_1}\right)\right) \\ i_{sd}\left(-\frac{2r}{L}\omega + \left(\frac{c_2}{c_1} + q\right)\omega\right) \\ + E_d\left(\frac{\omega}{L}\right) + V_{md}\left(\frac{-2\omega}{L}\right) + E_q\left(\frac{r}{L^2} - \left(\frac{c_2}{c_1} + q\right)\frac{1}{L}\right) \\ + V_{mq}\left(-\frac{r}{L^2} + \left(\frac{c_2}{c_1} + q\right)\frac{1}{L}\right) - \frac{1}{L}\frac{d}{dt}E_q \\ + \frac{d^2}{dt^2}x_{1ref} + \frac{d}{dt}x_{1ref}\left(\frac{c_2}{c_1} + q\right) + x_{1ref}\left(\frac{c_3}{c_1} + q\frac{c_2}{c_1}\right) \\ + q\frac{c_3}{c_1}\int\left(x_{1ref} - x_1\right)dt + \frac{\varepsilon}{c_1}Sgn(S_q) \end{bmatrix} \quad (18)$$

Therefore, we can obtain the instantaneous phase angle φ_i between the space vectors of grid voltages and input currents, such that

$$\varphi_i = tan^{-1}\left(\frac{i_{mq}}{i_{md}}\right) \quad (19)$$

where i_{md} is a modulated current; therefore, it cannot be sensed to compute in real-time Equ. (19). However, if the input filter losses are neglected, we can assume that the d-axis component of the line current i_{sd} is equal to i_{md}.

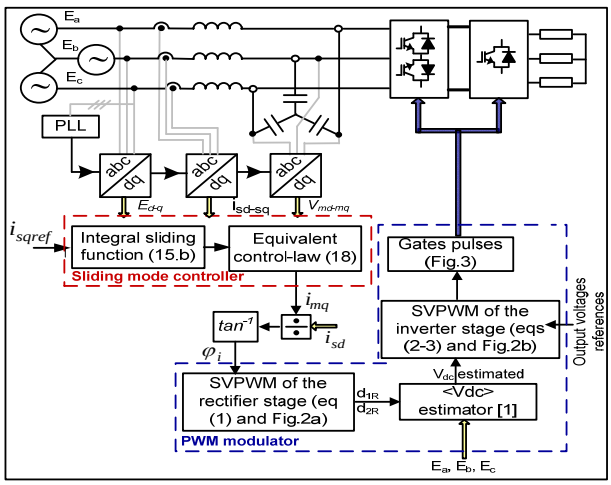

Fig. 4. Simplified block diagram of proposed PWM integral sliding-mode controller.

Consequently, Equ. (19) can be computed by replacing the term i_{md} with i_{sd} without loss of accuracy. Once φ_i is computed, we can determine the direction of the space vector of input current $\bar{I}_m^*$ and its phase angle within its respective operation sector $\bar{\gamma}_i$, as illustrated in Fig. 2(a). Once the direction of the space vector of input currents is determined, the DSVM technique is applied to compute the duty cycles d_{1R} and d_{2R} and synthesize the direction of $\bar{I}_m^*$. d_{1R} and d_{2R} are computed according to Equ. (1) given in Section II. As for the modulation of the target output voltages, we first estimate the local average value of the dc-link voltage $\langle V_{dc} \rangle$ in a similar manner, as performed in [1]. Thereafter, based on the amplitude and phase angle of the space vector of output voltages, we can compute the duty cycles for the inverter stage according to Equs. (2) and (3). Fig. 4 illustrates a simplified block diagram explaining the implementation principle of this control method. The grid and input filter capacitor voltages and the line currents are first reported into a dq reference frame using a phase-locked loop-based synchronization algorithm. Thereafter, the sliding-mode controller computes the control law $u_{eq} = i_{mq}$ according to Equs. (15b)-(18). The block PWM modulator computes the appropriate duty cycles of the rectifier and inverter stages according to Equs. (1)-(3) and Figs. 2(a-b). The appropriate gate pulses are also generated according to the switching strategy depicted in Fig. 3.

V. Simulation Results

A Matlab/Simulink numerical model of the IMC is developed to validate the proposed control method. The converter is built using the model of a metal-oxide-semiconductor field-effect transistor-type power transistor from the toolbox "simpowersystems" of Simulink. A three-phase voltage source system and a three-phase star-connected R-L branch are used to emulate the grid and load, respectively. All simulations are performed with a fixed step size equal to 1 µs. The parameters of the electrical system and the controller are reported in Table I.

TABLE I
Parameters Used for Simulation and Experimental Tests

Parameter Description	Assigned Values
Amplitude and frequency of grid voltage	E = 130 V (L-L), f= 60 Hz
Input passive filter	L = 2 mH, r = 0.5 Ω, C = 12 µF
R-L load	R_L= 12.5 Ω, L_L= 10 mH
Switching and sampling frequencies	f_{sw}= f_s= 8.5 kHz
Voltage transfer ratio	q = 0.75
Output frequency	f_o = 70 Hz
Sliding-mode controller	c_1 =1, c_2= 34.7, c_3= 2 10^6
Reaching law	q =1.66 10^2 , ε = 0.01 10^8

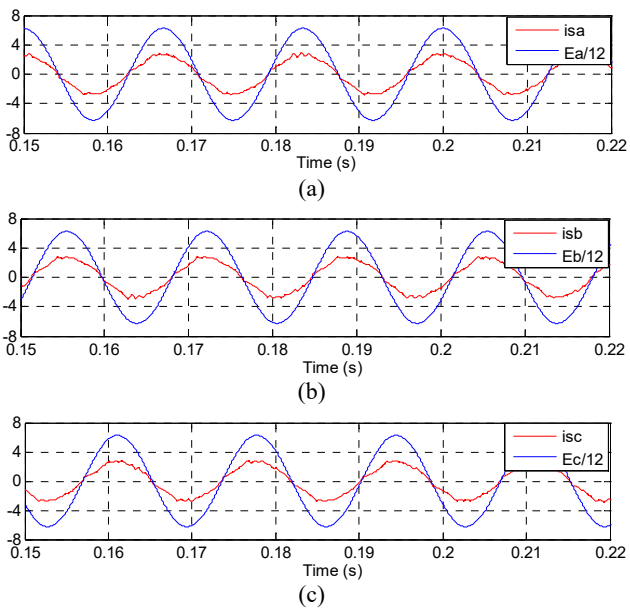

Fig. 5. Line-to-neutral grid voltages and currents (a) $E_a/12$ and i_{sa}- (b) $E_a/12$ and i_{sb} - (c) $E_c/12$ and i_{sc}.

Fig. 5 displays the steady-state waveforms of the line-to-neutral grid voltages and the line currents in the same phase. The three line currents are near in phase with their corresponding grid voltages, which implies that the converter operates effectively at near UIPF. This conclusion is emphasized by the result displayed in Fig. 6. The q-axis component of the line current (i_{sq}) varies around zero; this implies that the proposed sliding-mode controller enables the i_{sq} current to accurately track its target reference that is set to zero. Fig. 6 also shows that the waveform of the d-axis component of the line current (i_{sd}) is approximately constant, which means that a constant active power is being transferred to the load.

Figs. 7 and 8 display the line-to-line waveforms of output

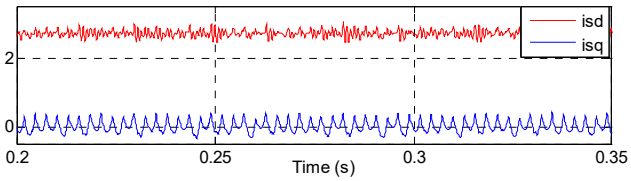

Fig. 6. Direct and quadrature components of the line current: i_{sd} and i_{sq}.

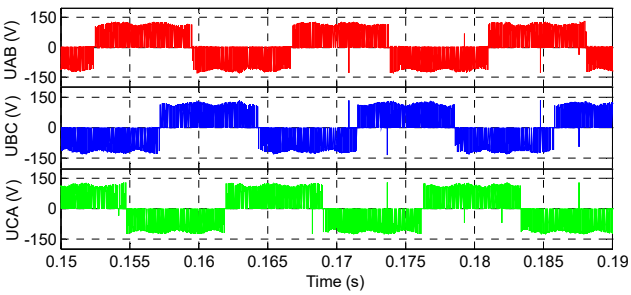

Fig. 7. Line-to-line output voltage (U_{AB} , U_{BC}, and U_{CA}) waveforms.

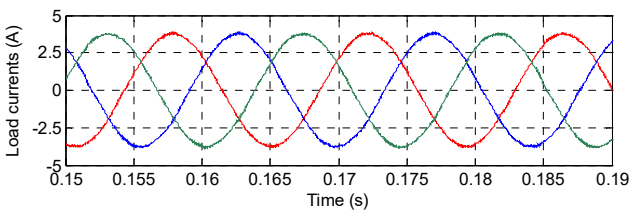

Fig. 8. Load current (i_A , i_B, and i_C) waveforms.

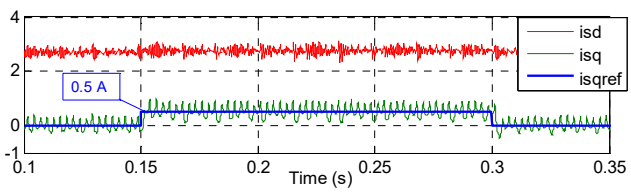

Fig. 9. d-axis and q-axis components of the line currents (i_{sd} and i_{sq}) with two abrupt changes in i_{sqref}.

voltages and load currents. The obtained currents are sinusoidal and balanced, thereby implying that the output voltages are correctly modulated.

Two abrupt changes in i_{sq} reference values are applied to evaluate the dynamic performance of the IMC with the proposed sliding-mode controller, as shown in Fig. 9. The first one is a step increase from $i_{sqref} = 0\,A$ to $i_{sqref} = 0.5\,A$, applied at time t = 0.15 s. The second one is a step decrease from $i_{sqref} = 0.5\,A$ to $i_{sqref} = 0\,A$, applied after 0.15 s. Fig. 9 depicts that a very fast dynamic response of i_{sq} is achieved with the sliding-mode controller, which also enables this current to follow perfectly its target reference i_{sqref} in both cases of step increase/decrease. The current i_{sd} is not affected by the variation of i_{sq}, which implies that the sliding-mode controller perfectly decouples the dynamics of i_{sq} and i_{sd}. Therefore, the IMC with the sliding-mode controller can inject an appropriate amount of reactive power into the grid without any impact on the active power

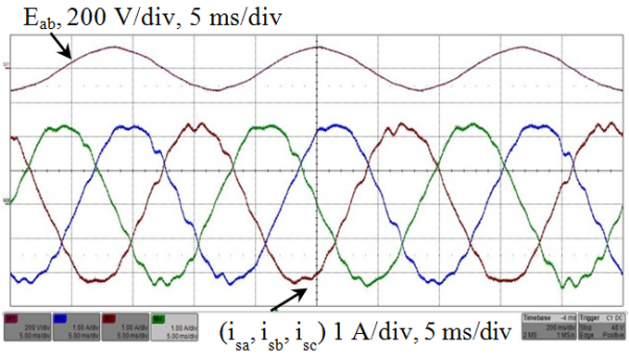

Fig. 10. Line-to-line grid voltage E_{ab} and line currents (i_{sa}, i_{sb}, i_{sc}).

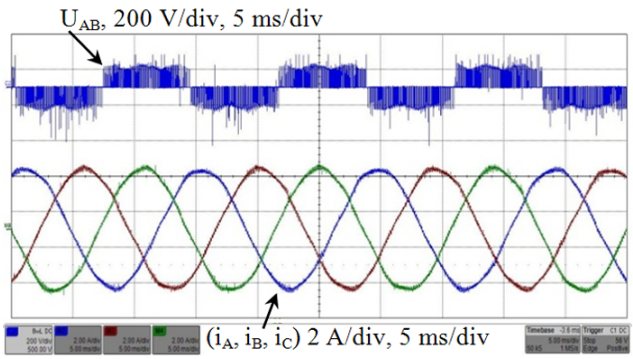

Fig. 11. Line-to-line output voltage U_{AB} and output currents (i_A, i_B, i_C).

transferred to the load.

VI. Experimental Results

The performance of the proposed control law is tested on a down-scale laboratory prototype of an IMC. The control and modulation algorithms are implemented on the DSP TMS320F28335 running at 150 MHz. The parameters of the electrical system and control algorithm are quite similar to those utilized in numerical simulations.

Fig. 10 displays the line-to-line grid voltage waveform (E_{ab}) and the line currents ($i_{sa,sb,sc}$), which are quite sinusoidal. Fig. 11 shows the line-to-line output voltage U_{AB} and the load currents (i_A,i_B,i_C), which draw a sinusoidal shape of fundamental frequency equal to 70 Hz. Only high-frequency ripple is observed in the waveforms of the load currents, which are inherently due to the switching operation of the converter. Fig. 12 illustrates the waveforms of the d- and q-axis components of the line currents (i_{sd} and i_{sq}). i_{sq} is varying in the vicinity of zero value. Therefore, a near UIPF is effectively achieved with this proposed control method. This statement is emphasized by the result in Fig. 13, which clearly shows that line current i_{sa} is in the phase with its corresponding grid voltage E_a. The total harmonic distortion (THD) of i_{sa} measured in real time is equal to 3.66%, which is lower than the limit value specified by the international standard IEEE-519. The high-frequency ripple

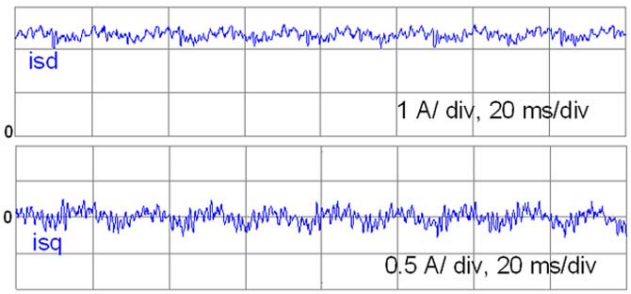

Fig. 12. d- and q-axis components of the line current (i_{sd}, i_{sq}).

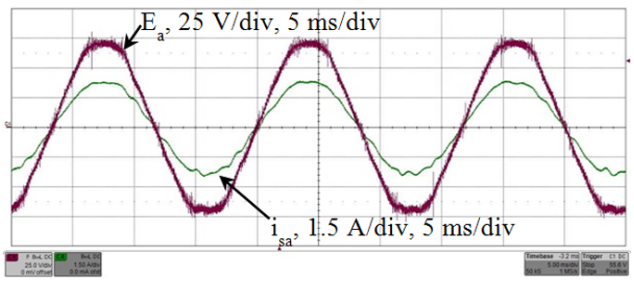

Fig. 13. Phase-to-neutral grid voltage E_a and current in the same phase i_{sa}.

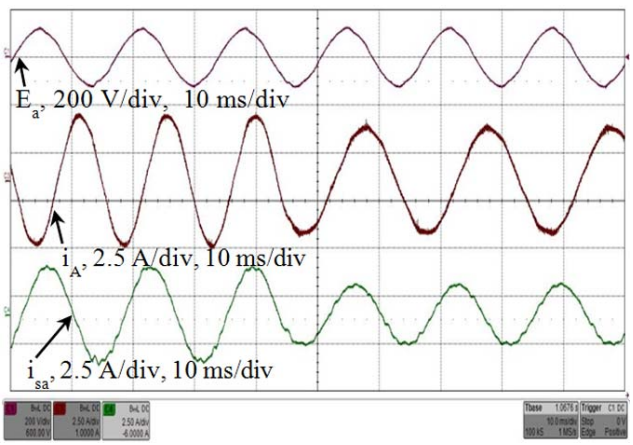

Fig. 14. Waveforms of the (top) line-to-line grid voltage, (middle) load current, and (bottom) line current under a step decrease in output frequency and voltage transfer ratio from $f_0 = 70\text{Hz}$ and $q = 0.75$ to $f_0 = 50\ \text{Hz}$ and $q = 0.6$, respectively.

appearing in the waveform of the phase-to-neutral grid voltage is mainly due to the common mode emissions that flow to the ground through the grid because no EMI filters are utilized.

Two step variations in the output frequency and the voltage transfer ratio are applied at the same time to examine the dynamic behavior of the proposed PWM-based integral sliding-mode controller. The output frequency and the voltage transfer ratio are abruptly changed from $f_0 = 70$ Hz and $q = 0.75$ to $f_0 = 50$ Hz and $q = 0.6$, respectively. Fig. 14 displays the load and line current waveforms during this transient regime. No observable oscillation occurs during this transient operation. Only the amplitude of both currents and the frequency of the load current are changed due to the

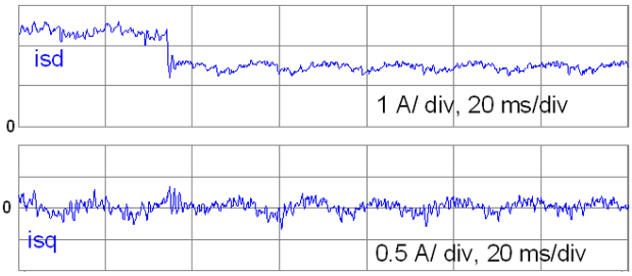

Fig. 15. d- and q-axis components of the line current (i_{sd}, i_{sq}) during the abrupt decrease in the output frequency and voltage transfer ratio.

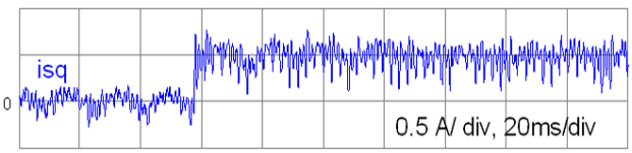

Fig. 16. q-axis component of the line current i_{sq} under an abrupt increase in its reference i_{sqref} from 0 A to 0.5 A.

variations in q and f_0. Fig. 15 shows that despite the decrease in the amplitude of the line current d-axis component, i.e., the decrease in the active power fed to the load, the q-axis component remains equal to zero.

In a third test, the q-axis line current reference i_{sqref} is abruptly increased from 0 A to 0.5 A. Fig. 16 displays the waveform of i_{sq} that tracks accurately its new reference without any overshoot. This result confirms the highly dynamic performance of the IMC controlled with the proposed PWM sliding-mode controller. The matrix converter with this proposed control law can operate as a static compensator.

VII. Conclusion

In this study, a PWM-based integral SMC algorithm is designed and successfully implemented on an IMC. The simulation and experimental results confirm the high performance of the proposed algorithm, which allows UIPF operation in steady state and a fast dynamic response. High-quality line currents are also provided, in which the THD is kept under the limits specified by the IEEE-519 standard. The results show that the converter can operate as a static compensator by injecting an appropriate amount of reactive current into the grid. This feature is important because it helps support the grid during voltage sags. This control method can be applied with other matrix converter topologies, such as matrix rectifier, four-leg IMC, five-phase IMC, and dual-output IMC, without the need for any change.

Appendix: Sliding Parameter Selection

When the sliding mode takes place (after the reaching phase), the dynamic response of the system theoretically satisfies the condition $S(t) = 0$ and $\dot{S}(t) = 0$. The sliding

parameters can therefore be designed to fulfill the stability condition during the sliding-mode operation [21]– [26]. Using pole placement technique, the stability condition is satisfied by assigning negative values to the real parts of the two poles of the characteristic Equ. (15.b). By identifying poles p_1 and p_2 into Equ. (15.b) and imposing $c_1 = 1$, we obtain $c_2 = -(p_1 + p_2)$ and $c_3 = (p_1p_2)$. In practice, the values assigned to p_1 and p_2 are $-17.36 \pm i\ 1414$, which yield $c_2 = 34.7$ and $c_3 = 2\ 10^6$.

REFERENCES

[1] M. Hamouda, H. F. Blanchette, and K. Al-Haddad, "Unity power factor operation of indirect matrix converter tied to unbalanced grid," *IEEE Trans. Power Electron.*, Vol. 31, No. 2, pp. 1095-1107, Feb. 2016.

[2] L. Wei, and T. A. Lipo, "A novel matrix converter topology with simple commutation," in *Proc. IAS*, pp. 1749-1754, 2001.

[3] L. Huber, and D. Borojevic, "Space vector modulated three-phase to three-phase matrix converter with input power factor correction," *IEEE Trans. Ind. Appl.*, Vol. 31, No. 6, pp. 1234-1246, Nov/Dec. 1995.

[4] M. Hamouda, H. F. Blanchette, K. Al-Haddad, and F. Fnaiech, "An efficient DSP-FPGA-based real-time implementation method of SVM algorithms for an indirect matrix converter," *IEEE Trans. Ind. Electron.*, Vol. 58, No. 11, pp. 5024-5031, Nov. 2011.

[5] Q. Guan, P. Yang, Q. Guan, X. Wang, and Q. Wu, "A singular value decomposition based space vector modulation to reduce the output common-mode voltage of direct matrix converters," *Journal of Power Electronics*, Vol. 16, No. 3, pp. 936-945, May 2016.

[6] Y. D. Yoon and S. K. Sul, "Carrier-based modulation technique for matrix converter," *IEEE Trans. Power Electron.*, Vol. 21, No. 6, pp. 1691-1703, Nov. 2006.

[7] P. C. Loh, R. Rong, F. Blaabjerg, and P. Wang, "Digital carrier modulation and sampling issues of matrix converters," *IEEE. Trans. Power Electron.*, Vol. 24, No. 7, pp. 1690-1700, Jul. 2009.

[8] Q-H Tran and H-H Lee, "An effective carrier-based modulation strategy to reduce the switching losses for indirect matrix converters," *Journal of Power Electronics*, Vol. 15, No. 3, pp. 702-711, May 2015.

[9] M. Hamouda, H. F. Blanchette, and K. Al-Haddad, "A hybrid modulation scheme for dual-output five-leg indirect matrix converter," *IEEE Trans. Ind. Electron.*, Vol. 63, No. 12, pp. 7299-7309, Dec. 2016.

[10] M. Hamouda, F. Fnaiech, and K. AL-Haddad, "Input filter design for SVM dual-bridge matrix converters," in *Proc. ISIE*, pp. 797-802, 2006.

[11] A. K. Sahoo, K. Basu, and N. Mohan, "systematic input filter design of matrix converter by analytical estimation of RMS current ripple," *IEEE Trans. Ind. Electron.*, Vol. 62, No. 1, pp. 132-143, Jan. 2015.

[12] M. Milanovic and B. Dobaj, "Unity input displacement factor correction principle for direct AC to AC matrix converters based on modulation strategy," *IEEE Trans. Circuits Syst.*, Vol. 47, No. 2, pp. 221-230, Feb. 2000.

[13] H. M. Nguyen, H.H. Lee, and T.W Chun, "Input power factor compensation algorithms using a new direct-SVM method for matrix converter," *IEEE Trans. Ind. Electron.*, Vol. 58, No. 1, pp. 232-243, Jan. 2011.

[14] K. You, D. Xiao, M. F. Rahman, and M. N. Uddin, "Applying reduced general direct space vector modulation approach of AC–AC matrix converter theory to achieve direct power factor controlled three-phase AC–DC matrix rectifier," *IEEE Trans. Ind. Appl.*, Vol. 50, No. 3, pp. 2243-2257, May/Jun. 2014.

[15] M. Rivera, J. Rodriguez, B. Wu, J. R. Espinoza, and C. A. Rojas, "Current control for an indirect matrix converter with filter resonance mitigation," *IEEE Trans. Ind. Electron.*, Vol. 59, No. 1, pp. 71-79, Jan. 2012.

[16] M. Hamouda, F. Fnaiech, and K. Al. Haddad, "Control of the reactive line current provided by a Dual-Bridge Matrix Converter using the input-output feedback linearization approach," in *Proc. ISIE*, pp. 803-808, 2006.

[17] S. Pinto and J. Silva, "Sliding mode direct control of matrix converters," *IET Electr. Power Appl.*, Vol. 1, No. 3, pp. 439-448, May 2007.

[18] M. Cucuzzella, G. P. Incremona, and A. Ferrara, "Design of robust higher order sliding mode control for microgrids," *IEEE J. Emerg. Sel. Topics Circuits Syst.*, Vol. 5, No. 15, pp. 393-401, Sep. 2015.

[19] F. Dinuzzo and A. Ferrara, "Higher order sliding mode controllers with optimal reaching ," *IEEE Trans. Autom. Control*, Vol. 54, No. 9, pp. 2126–2136, Sep. 2009.

[20] S. Oucheriah and L. Guo, "PWM-based adaptive sliding-mode control for boost DC–DC converters," *IEEE Trans. Ind.electron.*, Vol. 60, No. 8, pp. 3291-3294, Aug. 2013.

[21] S. C. Tan, Y.M. Lai, C. K. Tse, and M. K. H. Cheung, "A fixed-frequency pulse-width-modulation based quasi-sliding mode controller for buck converters," *IEEE Trans. Power Electron.*, Vol. 20, No. 6, pp. 600-61, Nov. 2005.

[22] M. Hamouda, H. F. Blanchette, and K. Al-Haddad, "Indirect matrix converters' enhanced commutation method," *IEEE Trans. Ind. Electron.*, Vol. 62, No. 2, pp. 671-679, Feb. 2015.

[23] J. Liu, F. Xiao, W. Ma, X. Fan, and Wei Chen, "PWM-based sliding mode controller for three-level full-bridge DC-DC converter that eliminates static output voltage error," *Journal of Power Electronics*, Vol. 15, No. 2, pp. 378-388, Mar. 2015.

[24] W. Gao, Y. Wang, and A. Homaifa, "Discrete-time variable structure control systems," *IEEE Trans. Ind. Electron.*, Vol. 42, No. 2, pp. 117-122, Apr. 1995.

[25] S-C Tan, Y. M. Lai, and C. K. Tse, "Indirect sliding mode control of power converters via double integral sliding surface," *IEEE Trans. Power Electron.*, Vol. 23, No. 2, pp. 1379–1392, Mar. 2008.

[26] S.C. Tan, Y. M. Lai, and C. K. TSE, "A unified approach to the design of PWM based sliding mode voltage controller for basic DC–DC converters in continuous conduction mode," *IEEE Trans. Circuits Syst. I: Fundam. Theory Appl.*, Vol. 53, No. 8, pp. 1816–1827, Aug. 2006.

Lazhar Rmili received his B.Sc.A. and M.Sc.A degrees and Specialized Scientific Studies Certificate (CESS), all in electrical engineering, from the High School of Sciences and Technologies of Tunis (ESSTT) in Tunisia in 2000, 2008, and 2004, respectively. He received the highest academic-rank qualification (Agrégation) degree in Electrical Engineering in 2006. He was a "Technologue" of electrical engineering with the Department of Electrical Engineering, Higher Institute of Technology of Rades (ISET), Tunisia in September 2006. His fields of interest include power quality, active filters, and matrix converter.

Mahmoud Hamouda received his B.Sc.A., Agregation, M.Sc.A., and Ph.D. degrees, all in electrical engineering, from ENSET and the Ecole Superieure des Sciences et Techniques, University of Tunis, Tunisia, in 1995, 1996, 2004, and 2010, respectively. He received the HDR from the University of Sousse in 2017. He is currently an Associate Professor of electrical engineering with ISSAT at the University of Sousse, Tunisia. He is affiliated with Canada Research Chair in Electric Energy Conversion and Power Electronics, Ecole de Technologie Supérieure in Montreal, Canada. He is also a member of the research laboratory of LATIS, National Engineering School of Sousse, University of Sousse, Tunisia. His main research interests include renewable energy conversion systems, digital signal processor, and field-programmable gate array for embedded real-time control, unbalanced weak grid systems, and development of advanced controllers, such as nonlinear control of matrix, multilevel, multicellular, multiphase converters, and grid-connected converters.

Salem Rahmani received his B.Sc.A. and M.Sc.A degrees and Specialized Scientific Studies Certificate, all in electrical engineering, from the High School of Sciences and Technologies of Tunis in Tunisia in 1992, 1995, and 2001, respectively. He received the highest academic-rank qualification (Agrégation) degree in Electrical Engineering in 2001, as well as his Ph.D. and the highest academic qualification (Habilitation qualifications) degrees from the National Engineering School of Tunis in 2004 and 2010, respectively. In September 2002, he was an Assistant Professor at the Department of Electrical Engineering, High Institute of Medical Technologies of Tunis. Since the elaboration of his Ph.D. degree, he has been a member of the Research Group in Power Electronics and Industrial Control, École de Technologie Supérieure, University of Québec, Montreal, QC, Canada. His fields of interest include power quality, active filters, and resonant converters, including power converter topology, modeling, and control aspects.

Handy Fortin Blanchette received his B.Eng., M.Eng., and Ph.D. degrees in electrical engineering from École de Technologie Supérieure, Montreal, PQ, Canada in 2001, 2003, and 2010, respectively. From 1994 to 1997, he was engaged in industrial automation. From 1998 to 2000, he was with the Bombardier Transport-ETS Research Laboratory, where he worked on a high-power traction system. From 2001 to 2003, he was involved in the development of an electrical drive library for the Simulink (MATLAB) environment. From 2007 to 2010, he was with OPAL-RT Technologies, where he led central processing unit- and field-programmable gate array-based power electronics real-time simulation projects. From 2010 to 2011, he was a Visiting Scholar at the Center for Power Electronic and System, Virginia Polytechnic Institute. He is currently an Associate Professor of electrical engineering at the Ecole de Technologie Supérieure in Montreal. His current research interests include EMI prediction, circuit modeling, and high-density power converter packaging.

Kamal Al-Haddad received his B.Sc.A. and M.Sc.A. degrees from the University of Québec à Trois-Rivières, Canada in 1982 and 1984, respectively, as well as his Ph.D. degree from the Institut National Polytechnique, Toulouse, France in 1988. Since June 1990, he has been a Professor at the École de Technologie Supérieure, Montreal, QC, where he has been the holder of the senior Canada Research Chair in Electric Energy Conversion and Power Electronics since 2002. He has supervised more than 100 Ph.D. and M.Sc.A. students and co-authored more than 500 papers and 2 books. His fields of interest are in high-efficiency power electronic converters, active and hybrid filters, modular multilevel converter, multilevel converters, and active rectifiers, including packaging, modeling, control, and development of industrial prototypes. Prof. Al-Haddad is the President of IEEE IES, a fellow of the Canadian Academy of Engineering, an Associate Editor of *Transactions on Industrial Informatics*, and an IES Distinguished Lecturer.